Molecular dynamics studies of alanine racemase: A structural model for drug design

ARTICLE *in* BIOPOLYMERS · OCTOBER 2003

Impact Factor: 2.39 · DOI: 10.1002/bip.10425 · Source: PubMed

3 AUTHORS:

Gabriela Mustata Wilson
University of Southern Indiana
36 PUBLICATIONS **527** CITATIONS
SEE PROFILE

Thereza A Soares
Federal University of Pernambuco
53 PUBLICATIONS **820** CITATIONS
SEE PROFILE

James M Briggs
University of Houston
95 PUBLICATIONS **4,148** CITATIONS
SEE PROFILE

Gabriela Iurcu Mustata[1]
Thereza A. Soares[2]
James M. Briggs[1]
[1] *Department of Biology and Biochemistry, University of Houston, Houston,TX 77204-5001*

[2] *Institute of Physical Chemistry, ETH Hoenggerberg, HCI G223, CH-8093 Zürich, Switzerland*

Received 9 October 2002; accepted 28 February 2003

Molecular Dynamics Studies of Alanine Racemase: A Structural Model for Drug Design

Abstract: *Alanine racemase (AlaR) is a bacterial enzyme that catalyzes the interconversion of* L- *and* D-*alanine, which is an essential constituent of the peptidoglycan layer of the bacterial cell wall and requires pyridoxal 5′–phosphate (PLP) as a cofactor. The enzyme is universal to bacteria, including mycobacteria, making it an attractive target for drug design. To investigate the effects of flexibility on the binding modes of the substrate and an inhibitor and to analyze how the active site is affected by the presence of the substrate versus inhibitor, a molecular dynamics simulation on the full AlaR dimer from* Bacillus stearothermophilus *(pdb code: 1SFT) with a* D-*alanine molecule in one active site and the noncovalent inhibitor, propionate, in the second site has been carried out. Within the time scale of the simulation, we show that the active site becomes more stabilized in the presence of substrate versus inhibitor. The results of this simulation are in agreement with the proposed mechanism of alanine racemase reaction in which the substrate carboxyl group directly participates in the catalysis by acting cooperatively with Tyr 265′ and Lys 39. A structural water molecule in contact with both substrate and inhibitor (i.e., in both active sites) and bridging residues in both active sites was identified. It shows a remarkably low mobility and does not exchange with bulk water. This water molecule can be taken into account for the design of specific AlaR inhibitors by either utilizing it as a bridging group or displacing it with an inhibitor atom. The results presented here provide insights into the dynamics of the alanine racemase in the presence of substrate/inhibitor, which will be used for the rational design of novel inhibitors.* © 2003 Wiley Periodicals, Inc. Biopolymers 70: 186–200, 2003

Keywords: *alanine racemase; molecular dynamics; essential dynamics*

INTRODUCTION

Alanine racemase (AlaR) catalyzes the interconversion of L- and D-alanine (D-Ala), providing the latter enantiomer for the construction of the peptidoglycan layer of the bacterial cell wall. All known bacteria require D-Ala, whereas only L-alanine is used in mammalian protein synthesis. Presumably, specific inhib-

Correspondence to: James M. Briggs; email: jbriggs@uh.edu
Contract grant sponsor: NSF; Contract grant number: ACI-9619020
Contract grant sponsor: NIH; Contract grant number: AI46340
Biopolymers, Vol. 70, 186–200 (2003)

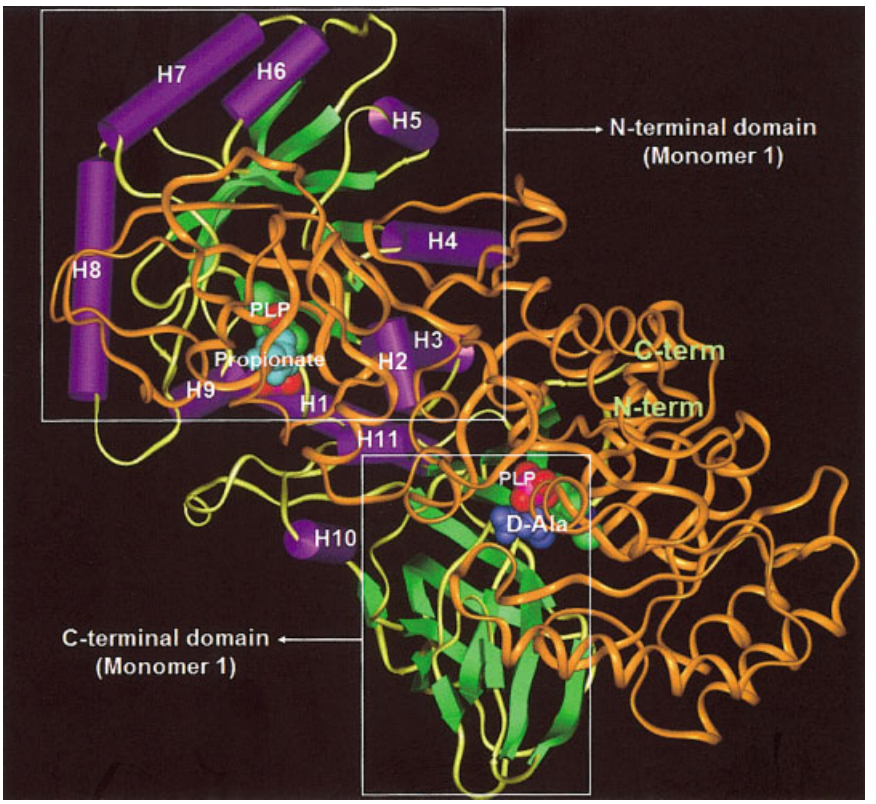

FIGURE 1 Pictorial view of the *Bacillus stearothermophilus* alanine racemase homodimer. The first monomer is rendered following the Kabsch-Sander classification; the PLP cofactor is rendered in CPK and colored by atom; propionate is rendered in CPK and colored in turquoise. The second monomer is displayed in ribbon and colored in orange; the PLP cofactor is rendered in CPK and colored by atom; D-Ala is rendered in CPK and colored in blue. The N-terminal domain (α/β barrel; residues 1–240) and the C-terminal domain (residues 241–382) of the first monomer are indicated by white boxes. The numbering of the α helices from the α/β barrel is in accordance with the one published by Shaw et al.[8]

itors of AlaR would kill bacteria but have no adverse side effects, because there are no known mammalian AlaRs. A number of effective inhibitors of AlaR have been developed.[1–4] However, most of these compounds are nonspecific suicide inhibitors that react with the cofactor itself, inhibiting the activity of many pyridoxal 5′–phosphate (PLP)-containing enzymes. These inhibitors form a covalent link either with the cofactor or, ultimately, with the enzyme.

AlaR's catalytic activity depends on the binding of the cofactor PLP, a phosphorylated and oxidized form of vitamin B6. PLP binds covalently to the protein by means of an imine bond to the ϵ-amino group of the side chain of a lysine, which is commonly designated as the internal aldimine (Schiff's base) form.[5] The amine group of the substrate alanine displaces the Schiff's base in a transaldimination reaction, forming the reactive external aldimine intermediate. Deprotonation of the α-carbon leads to the formation of a planar α-carbanion intermediate, which is resonance-stabilized by the pyridoxal phosphate ring.[6,7] This intermediate then undergoes reprotonation on either face of the planar intermediate to generate either enantiomer of alanine. Recent experimental[8–10] and theoretical data[11] support a two-base mechanism for the catalytic function of AlaR where Lys 39 and Tyr 265′ could act as catalytic bases.[10,11]

Five crystallographic structures of AlaR from *Bacillus stearothermophilus* have been reported so far, including the complexes between AlaR and two inhibitors, namely propionate and 1-aminoethylphosphonic acid.[6,8–10] The crystal structure revealed that the enzyme is a homodimer (Figure 1) of 388 residues.[8] Each monomer is composed of two folded domains, an N-terminal domain from residues 1–240 and a C-terminal domain from residues 241–388. The N-terminal domain is made up of an eight-stranded α/β-barrel and the C-terminal domain mainly of β-strands. The active form of AlaR is a homodimer, such that the active site is formed by the mouth of the

α/β-barrel of one monomer and the C-terminal domain of the other monomer. The active site of AlaR is composed of PLP, which is crosslinked to Lys 39 via a protonated Schiff's base linkage, and the amino acids in the immediate environment of the PLP. Several residues from the other monomer, namely, Tyr 265′, Met 312′, Asp 313′, and Gln 314′, are close to the cofactor and might play a role in binding or catalysis.[8]

In an effort to understand the structural determinants for the binding of the D-Ala substrate, as well as the noncovalent inhibitor propionate, a molecular dynamics (MD) simulation was performed on the full length *B. stearothermophilus* AlaR dimer. Site directed mutagenesis studies demonstrated that the two active sites of AlaR from *E. coli* and *Pseudomonas aeruginosa*, which share more than 85% identity with *B. stearothermophilus* AlaR, do not interact (i.e., there is no cooperativity between the two active sites).[12] Based on this experimental evidence and considering the fact that there are very few obvious polar interactions at the interface between monomers and that the active sites are far apart (ca. 30 Å),[8] we performed an MD simulation on the full dimer with a different ligand bound to each active site. In this way we could obtain twice the amount of information from a single simulation (i.e., that for an active site with an inhibitor and one with a substrate, D-Ala).

The information gleaned from these studies is a prerequisite to subsequent steps of structure-based design of specific inhibitors taking into account protein flexibility. Our aim is to develop a "dynamic" pharmacophore model for AlaR, which would allow the determination of pharmacophore features that complement the protein's active site taking into account native receptor flexibility. This is generally accomplished by analyzing small molecule binding sites or property volumes in multiple conformations of the protein to identify conserved pharmacophore elements. The main motivation in developing a dynamic pharmacophore is based on the fact that in the case of HIV-1 integrase, known inhibitors were identified from small molecule databases using a dynamic pharmacophore model, but not with the commonly used static model (i.e., a pharmacophore model based on a single receptor structure, typically the x-ray or NMR structure).[13]

RESULTS AND DISCUSSION

The results reported here are based on a 2 ns trajectory of the AlaR homodimer with the noncovalent inhibitor propionate in one active site and a D-Ala substrate in the second one (see Methods). The temperature, total energy, mass density, and volume remained stable during the 2 ns trajectory. The temperature and total potential energy were inspected to ensure the stability of the trajectory.

Global Structural Stability

As a measure of structural stability, the root-mean-square deviations (RMSDs) of C_α atoms of individual conformations of AlaR were computed along the 2 ns trajectory (Figure 2). This RMSD, measured relative to the minimized crystal structure conformation, has a value of about 0.75 Å at the beginning of the trajectory, indicating that movements away from the crystal structure have occurred during the thermalization and equilibration periods that precede the production run. Thereafter, only a small overall drift is observed, with fluctuations of the order of 0.35 Å during the 2 ns trajectory, indicating a stable protein structure. The backbone RMSD of the average protein conformation with respect to the minimized crystal structure computed from the entire 2 ns trajectory is 1.20 Å, and that of the all atoms (including aliphatic hydrogens) is 1.35 Å. From Figure 2 we can see that the RMSD of the PLP cofactor, covalently linked to Lys 39, is very stable for the entire simulation, leveling off to 0.8 Å. The RMSD of the substrate (D-Ala) with respect to its starting position remains below 0.15 Å for the first 1.4 ns of the trajectory, reaching 0.25 Å in the last part of the simulation. On the other hand, the RMSD of the inhibitor (propionate) occasionally reaches 1 Å, although it remains around 0.4 Å for most of the simulation. The movement of the substrate/inhibitor is strongly correlated, as we show later in this section, with the distances between the ligand and active site residues.

The protein does not undergo significant unfolding processes, as evidenced by the stable radius of gyration (data not shown) and by the secondary structure content calculated during the simulation. The secondary structure analysis carried out using the DSSP[14] algorithm shows conservative structural elements with respect to the crystal structure. The only noticeable change occurs in the N-terminal domain of the first monomer. The α-helix H10 and the β-sheet B1 are both shortened by two residues, and adopt a turn and a coil conformation during the MD simulation. These residues are distant from the active site and not involved in the catalytic activity. They are, however, located within flexible regions of the protein. H10 is one of the two short helices that are part of the C-terminal domain, and B1 is situated at the extreme of the N-terminal end of the protein.

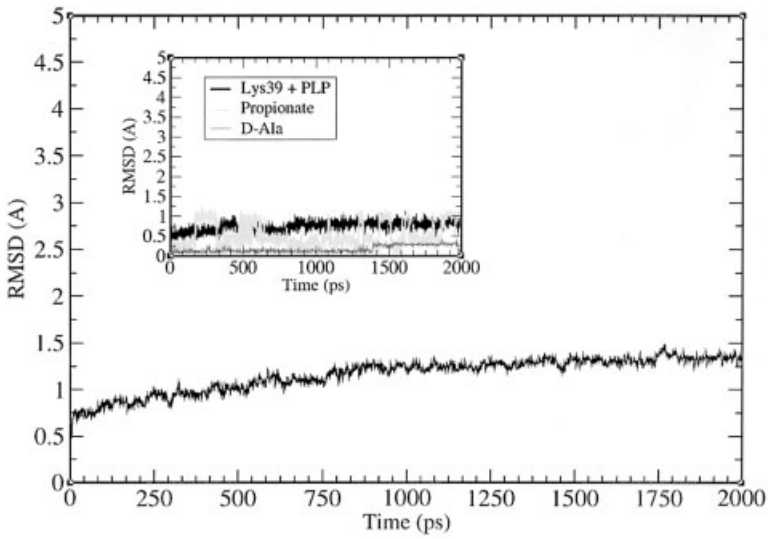

FIGURE 2 The RMSD of the C_α atoms as a function of the simulation time. Values correspond to snapshot structures separated by 0.5 ps along the 2 ns trajectory. The inset figure shows the RMSD for the substrate (D-Ala) (dashed gray line), the inhibitor (propionate) (dashed light gray line), and Lys 39 covalently linked to the PLP cofactor (solid black line).

Other properties such as the solvent accessible surface area (SASA) were also monitored along the trajectory (Figure 3). We can see no significant change in protein accessible surface area (hydrophobic and hydrophilic) during the 2 ns production run. Considering all of the simulation phases, the largest change relative to the crystal structure is 11.8% for the hydrophobic and 12.3% for the hydrophilic parts. In general, the surface area changes result from movements of surface side chains and the N-terminus, which lead to their increased exposure. The fluctuation of the surface area of individual conformations relative to the average values of the corresponding quantity, evaluated over the entire trajectory, is significantly smaller and does not exceed 2.2%.

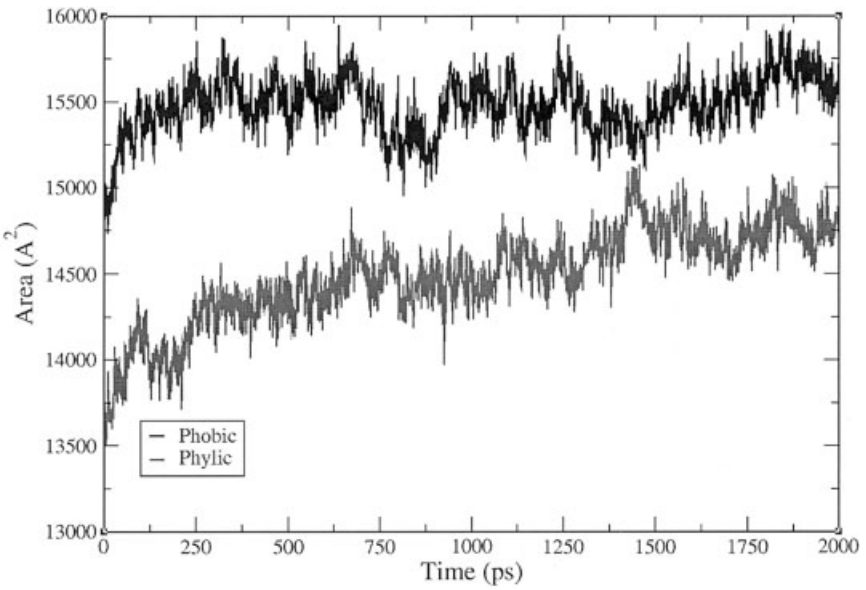

FIGURE 3 Accessible surface areas (hydrophobic and hydrophilic) (Å^2) of AlaR along the 2 ns trajectory. The values corresponding to the accessible surface area of the refined crystal structure are 14,232 Å^2 (hydrophobic) and 13,206 Å^2 (hydrophilic).

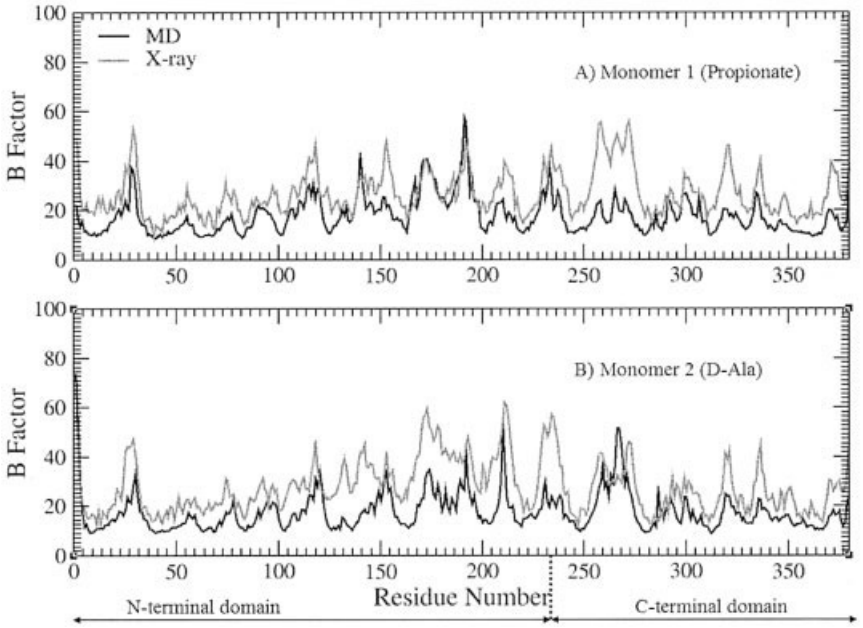

FIGURE 4 Comparison of B-factors of C_α atoms calculated from the 2 ns MD trajectory and from the energy minimized x-ray structure of AlaR. The ordinate shows B-factor magnitudes in units of $Å^2$. The abscissa shows residue numbers in the first monomer (propionate in the active site) (A), and in the second one (D-Ala in the active site) (B). The N-terminal domain (residues 1–240) and C-terminal domain (241–382) are indicated.

In Figure 4, a comparison between the C_α x-ray B-factors and the computed ones from the 2 ns MD simulation is shown. As can be seen, the computed B-factors generally display a lower base level, although the overall profile of the MD data is in agreement with the regions that have the largest B-factors in the x-ray structure. The isotropic temperature factors also provide a means of finding out which parts of the protein are behaving differently, in our case, one monomer as compared to the other in the homodimer. From Figure 4 we can observe that the second half of the N-terminal domain (residues 100–240) in both monomers displays larger computed B-factors as compared to the ones displayed by the residues from the first half of the same domain. These fluctuations are to some degree larger for the first monomer. Interestingly, the computed B-factors are larger in the first half of the C-terminal domain of the second monomer as compared to the ones from the first monomer. Because each active site is mainly composed of residues that belong to the second half of the N-terminal domain of one monomer, as well as residues that belong to the first half of the C-terminal domain of the opposite monomer, we do have the indication that the first active site (propionate present) shows higher flexibility than that with the substrate D-Ala bound.

Structural Changes of One Monomer Relative to the Other

Fluctuations of the C_α Atoms. The fluctuations averaged over the C_α atoms $\langle d_{C_\alpha} \rangle$ of both AlaR monomers are presented in Table I, along with the correlation coefficients between the fluctuations. Usually, the magnitude of the fluctuations permits the identification of stable secondary structures from the disorganized ones, the latter featuring higher fluctuations than those of the former. We can see that the magni-

Table I Average Fluctuations of C_α Atoms and Correlation Coefficients

	Monomer 1 (Propionate)		Monomer 2 (D-Ala)	
	All Residues	Active Site Residues	All Residues	Active Site Residues
$\langle d_{C_\alpha} \rangle$ (Å)	0.69	0.73	0.68	0.61
$r(d_{C\alpha})$	—	—	0.57	0.813

($d_{C\alpha}$) is the average atomic fluctuation (in Å) averaged over the C_α atoms.

$r(d_{C\alpha})$ is the correlation coefficient of the C_α atom fluctuations between the two monomers/active sites, computed using the SAS package.[39]

tude of $\langle d_{C_\alpha} \rangle$ is similar for both monomers and moderately larger in the case of the first active site (propionate present) as compared to the second active site (D-Ala present). The C_α fluctuations in the two monomers are only correlated with a correlation coefficient of 0.57. Residues of the two active sites correlate better, with a correlation coefficient of 0.81. Note that each active site is composed mainly of residues from one monomer and several residues from the other monomer that are close to the PLP cofactor (e.g., Tyr 265′, Met 312′, Asp 313′, and Gln 314′). The average atomic fluctuation averaged over the C_α atoms of the active site residues of the first monomer (propionate in the active site) is 0.73 Å, while the one for the active site residues of the second monomer (D-Ala in the active site) is 0.61 Å. This indicates that the active site becomes slightly more stabilized in the presence of the substrate (D-Ala) as compared to the inhibitor (propionate). The residues that seem to be responsible for this are Arg 136 and Tyr 265′: the RMSF of Arg 136 is 0.94 Å in the active site with the bound propionate versus 0.45 Å in the active site with the bound substrate, and the RMSF of Tyr 265′ is 1.35 Å in the active site with the bound propionate versus 0.71 Å in the active site with the bound substrate.

Solvent Accessibilities. The SASA of the side chains of residues of the active sites was computed in every snapshot along the 2 ns trajectory and the average values were normalized by a standard value of the corresponding residue in an extended Gly-XXX-Gly tripeptide (where XXX = the residue of interest) with the side chain in an extended conformation with standard bond lengths and angles[16] (Table II). We can see that the fraction of the surface being exposed to the solvent for the residues that are part of the second active site (D-Ala present) is larger than the one corresponding to the same residues from the first monomer (propionate in the active site). Notably, however, a few side chains (His 166, Tyr 265′, and Gln 314′) display a relatively larger SASA (see Table II) in the propionate-bound active site.

Table II Normalized Solvent-Accessible Surface Area (NSASA)[a] of the Most Important Active Site Residues, Averaged over the 2 ns Trajectory

Residue	Active Site 1 (Propionate)	Active Site 2 (D-Ala)
Lys 39	0.04	0.15
Tyr 43	0.00	0.12
Lys 129	0.00	0.00
Arg 136	0.02	0.01
His 166	0.08	0.05
Arg 219	0.01	0.00
Tyr 265′	0.04	0.03
Met 312′	0.00	0.14
Asp 313′	0.07	0.17
Gln 314′	0.12	0.05
Tyr 354	0.03	0.19

[a]For any given residue, there is a theoretical maximum solvent-accessible surface area that was computed for the Gly-XXX-Gly tripeptide (XXX = residue of interest) with the side chain in an extended conformation with standard bond lengths and angles.[16] The NSASA represents the fraction of the surface being exposed (computed exposed/theoretical maximum).

Side Chain Mobility. The computed average fluctuation of the side chain torsion angles χ_1 and χ_2, which are the most constrained angles due to their closeness to the main chain, provides information on the degree of side chain flexibility. Fluctuations in χ_1 and χ_2

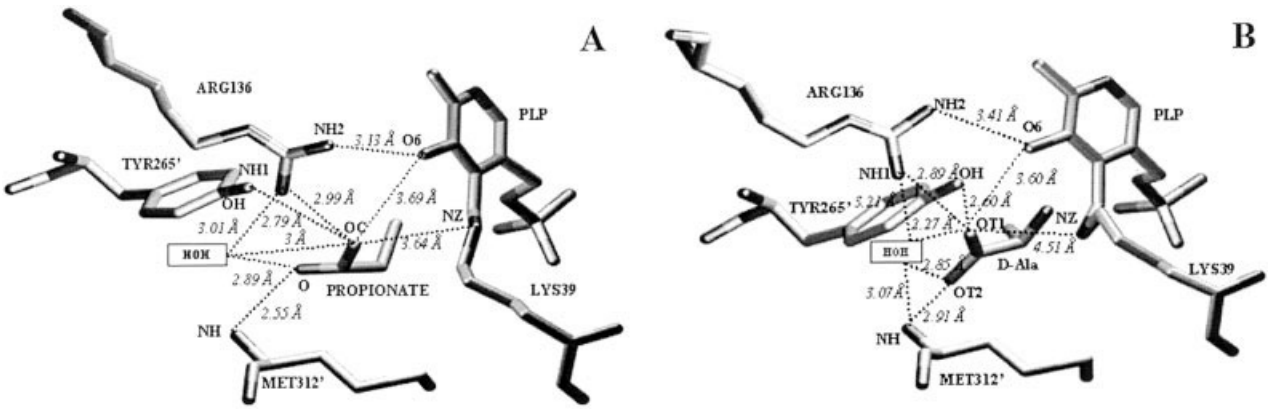

FIGURE 5 (A) Schematic diagram of interactions made by the propionate inhibitor with active site residues.[6] (B) Schematic diagram of interactions made by the D-Ala substrate. Residues labeled with a prime are from the other monomer.

Table III X-Ray Distance, Average Distance (Å), and RMSF for the Interactions between the Propionate Inhibitor and Active Site Residues, from the X-Ray Structure and the Entire 2 ns Trajectory

Interactions	X-Ray Distance (Å)	MD Average Distance (Å)	RMS Fluctuation (Å)
Arg 136 NH1 . . . OC-Propionate	2.99	3.42	0.42
Tyr 265′ OH . . . OC-Propionate	2.79	6.63	1.44
Lys 39 NZ . . . OC-Propionate	3.64	4.03	0.72
HOH . . . OC-Propionate	3.00	3.11	0.44
Met 312′ NH . . . OC-Propionate	2.55	3.49	0.51
HOH . . . OC-Propionate	2.89	2.92	0.48
Arg 136 NH1 . . . HOH	3.01	3.77	0.33
Arg 136 NH2 . . . O6PLP	3.13	3.54	0.48
Arg 313′ NH . . . HOH	3.03	2.95	0.17

higher than 25° are frequently observed in both monomers, but do not appear to differ significantly between the two monomers (data not shown). However, χ_1 and χ_2 angles in the first active site (propionate present) exhibit somewhat larger fluctuations than those of the second active site (D-Ala present). The most noticeable differences were observed for the side chain torsion angle χ_1 of His 166, Tyr 265′, and Gln 314′. These residues (i.e., in the first active site) display fluctuations that are about twice as large as the corresponding ones from the second active site, and have a relatively larger SASA (see Table II). Thus, in general, the stabilization of the second active site with the bound substrate appears to be reflected in the behavior of the side chains. When the substrate binds, the side chains along the active site region become more rigid than when the inhibitor binds. This might suggest that flexibility in the propionate-bound active site region may allow accommodation of different types of inhibitors.

Interactions between the Propionate/D-Ala and Active Site Residues. The structure of the propionate-bound active site described by Morollo et al.[6] shows a number of features unique to AlaR as compared to other PLP-dependent enzymes. That is, AlaR uses several types of interactions to stabilize the substrate carboxylate group (Figure 5A), such as the residue side chains of Arg 136 and Tyr 265′, the main chain of Met 312′, and the phenolic oxygen of PLP. These interactions were monitored during the 2 ns trajectory in order to determine the influence of the inhibitor/substrate on the structural and dynamical properties of the active site region. The interactions made by the inhibitor/substrate and the active site residues along the 2 ns trajectory are given in Table III and IV.

From Table III we can see that in the case of the inhibitor-bound active site almost all of the interactions remained within hydrogen bond distance for the entire length of the simulation, with the exception of one interaction, that between the OH of Tyr 265′ and

Table IV X-Ray Distance, Average Distance (Å), and RMSF for the Interactions between the D-Ala Substrate and Active Site Residues, from the X-Ray Structure and the Entire 2 ns Trajectory

Interaction	X-Ray Distance (Å)	MD Average Distance (Å)	RMS Fluctuation (Å)
Arg 136 NH1 . . . OT1-D-Ala	2.89	3.37	0.28
Tyr 265′ OH . . . OT1-D-Ala	2.60	2.73	0.15
Lys 39 NZ . . . OT1-D-Ala	4.51	5.12	0.35
HOH . . . OT1-D-Ala	2.27	3.43	0.48
HOH . . . OT2-D-Ala	2.85	3.40	0.58
Met 312′ NH . . . OT2-D-Ala	2.91	3.28	0.37
Met 312′ NH . . . HOH	3.07	3.29	0.26
Arg 136 NH1 . . . HOH	3.21	3.45	0.43
Arg 136 NH2 . . . O6PLP	3.41	3.07	0.23
Asp 313′ NH . . . HOH	2.84	3.22	0.57

the carboxylate oxygen, OC, of the propionate. This hydrogen bond remained intact only at the beginning of the simulation (2% presence along the 2 ns trajectory). This is different in the case of the substrate-bound active site (see Table IV). The corresponding interaction (Tyr 265′ OH–OT1-D-Ala) remained stable for the entire trajectory with a very small RMSF (0.15 Å) for the entire MD simulation. This is an indication, and supports the hypothesis made by Watanabe et al.,[10] that the substrate carboxyl group participates in catalysis by acting cooperatively with Lys 39 and Tyr 265′. On the contrary, this is not the case for the propionate carboxyl group.

The two stabilizing interactions involving the carboxylate group of the inhibitor,[6] that is, the interaction between the backbone amide N of Met 312′ and the carboxylate oxygen, O, of the inhibitor, and the interaction between the second carboxylate oxygen, OC, of propionate and the NH1 of Arg 136, remained well preserved for the entire trajectory. These interactions are also well maintained in the second active site with the bound substrate (see Table IV; the interaction between the backbone amide N of Met 312′ and the carboxylate oxygen, OT2, of D-Ala, and the interaction between the second carboxylate oxygen of D-Ala, OT1 and the NH1 of Arg 136).

It has been shown that Arg 136 appears to be involved in carboxylate binding in a manner that is unusual in other PLP-dependent enzymes.[6] That is, Arg 136 forms a bridge between one carboxylate oxygen (OC) of propionate and also bridges the PLP ring through a hydrogen bond with the phenolic oxygen (O6) (see Figure 5A). This residue is basically bridging both the inhibitor and the PLP ring. This appears to be also the case in the second active site with the bound substrate (Figure 5B). These hydrogen bonds are well preserved in both active sites during the entire MD simulation with larger RMSFs in the case of propionate as compared to the substrate D-Ala (see Table III and IV). Therefore, as Stamper et al.[9] suggested, and corroborated by the fact that the interaction between Arg 136 and the phenolic oxygen of the PLP cofactor is within hydrogen bonding distance for the entire length of our simulation, we have shown that this interaction is important in positioning the substrate relative to the cofactor.

Besides these interactions, a water molecule was found to be conserved in both active sites. This water molecule is in contact with both the substrate and inhibitor in each active site (see Figure 5A and B), and is hydrogen bonded to NH1 of Arg 136 and the carboxylate group of the substrate/inhibitor. These hydrogen bonds were monitored during the 2 ns trajectory and were found to remain well preserved (see Table III and IV). In addition to this, the water molecule bridges residues Arg 136, Met 312′, and Asp 313′ in the second active site and shows a remarkably low mobility and does not exchange with bulk water (Table IV). On the contrary, the corresponding water molecule from the first active site (propionate present) is bridging only two hydrogen bonds with residues Arg 136 and Asp 313′ (Figure 5A). These hydrogen bonds are also well preserved during the entire MD simulation. However, the fact that there are fewer water-mediated hydrogen bonds in the first active site might explain why the substrate-bound active site appears to be more stable as compared to the one with the bound inhibitor. Nevertheless, this structural water molecule with a high-residence time can be taken into consideration by displacing with an atom/group in a designed inhibitor.

Characteristic Features of the Active Sites

As we previously mentioned, the active site of AlaR is composed of the PLP cofactor, which is covalently linked to Lys 39, and the amino acids in the immediate environment of the pyridoxal cofactor. In order to obtain another measure of the dynamics of the active sites, distances across the active site in both monomers have been calculated and are displayed in Table V. The distance between Val 37 and Tyr 265′ determines the width of the active site, and the distance between Leu 85 and Met 312′ determines the height of the active site. Finally, the distance between Tyr 354 and Ile 309′ defines the depth of the active site pocket. The width of the first active site (propionate present) is to some degree larger than the one of the second active site, while the height and the depth are moderately larger in the case of the substrate-bound active site. From Figure 6 and Table V we can see that the width of the first active site increases, mainly due to the side chain flexibility of Tyr 265′. No significant changes were observed in the other two distances. This is another indication that the active site becomes more stabilized in the presence of the substrate, D-Ala, versus the noncovalent inhibitor propionate. Moreover, the molecular volume of each active site cavity, computed with CASTp[17] using the average structure from the 2 ns MD trajectory, shows that the active site cavity with the bound propionate is almost 20% larger than the substrate-bound active site; 2176 $Å^3$ for the propionate-bound active site versus 1754 $Å^3$ for the D-Ala-bound active site (the calculation was performed after removing all waters as well as inhibitor/substrate from the active sites). This information is very useful for structure-based drug design because,

Table V Comparison of Distances (Å) across the Active Sites

	Active Site 1 (Propionate)			Active Site 2 (D-Ala)		
Interaction	X-Ray Distance (Å)	MD Average Distance (Å)	RMS Fluctuation (Å)	X-Ray Distance (Å)	MD Average Distance (Å)	RMS Fluctuation (Å)
Val 37:CG1-Tyr 265′:OH	17.22	20.84	1.97	16.13	16.69	0.36
Leu 85:CD1-Met 312′:CE	9.08	9.21	0.50	9.63	10.19	0.83
Tyr 354:OH-Ile 309′:O	10.22	10.44	0.50	10.83	10.89	0.43

The X-ray distance, the average distance, and the RMSF during the 2 ns simulation are indicated for both active sites.

The distance between Val 37 and Tyr 265′ determines the width of the active site; the distance between Leu 85 and Met 312′ determines the height of the active site; the distance between Tyr 354 and Ile 309′ defines the depth of the active site pocket.

based on these results, one would obviously decide to focus on the active site with the bound inhibitor because it is larger. This choice is governed not only by the fact that the active site is larger but also because taking into account protein flexibility upon inhibitor binding should be more meaningful for drug design purposes.

Essential Dynamics (ED) Properties

An ED analysis[18] was applied to the 2 ns trajectory, using the GROMACS 3.0 program.[19] This method was used to evaluate similarities and differences between essential (i.e., correlated) motions of the two monomers along the 2 ns trajectory. Only a few eigenvectors were found to represent the essential motions in the protein. The components of the first eight eigenvectors are displayed in Figure 7. The eigenvectors show that correlated motions exist between the two monomers. However, there are some regions in each monomer that are more flexible (i.e., they have larger displacements) than others. Larger deviations in the N-terminal domain (α/β barrel) of the first monomer, as compared to the same domain of the second monomer, are also observed.

Table VI shows the displacements for the active site residue averaged over the first eight eigenvectors for the entire MD trajectory. It can be seen that the residues of the first active site (propionate present) are more flexible (i.e., they have larger displacements)

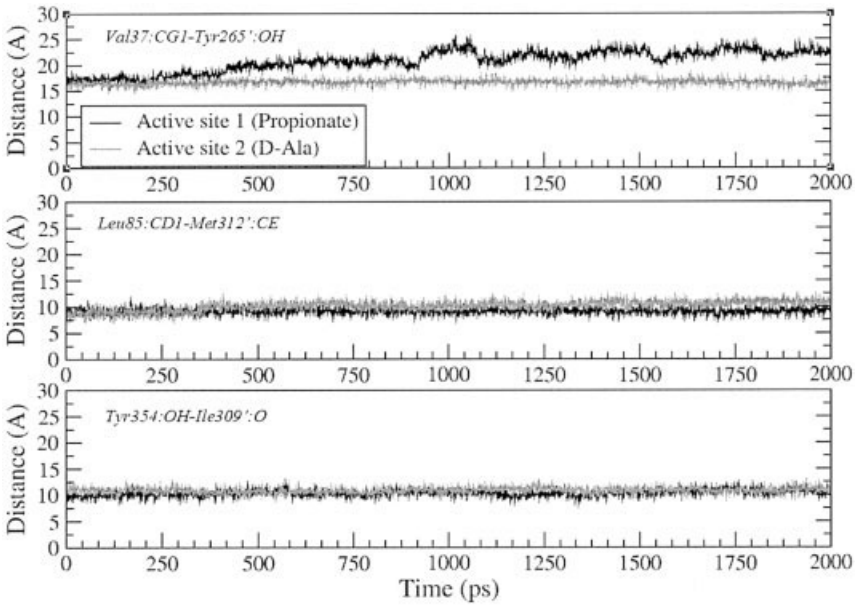

FIGURE 6 Distances across the active sites measured along the 2 ns trajectory. Residues of the first monomer (propionate in the active site) are represented with a thick solid line; residues of the second monomer (D-Ala in the active site) are represented with a dashed line.

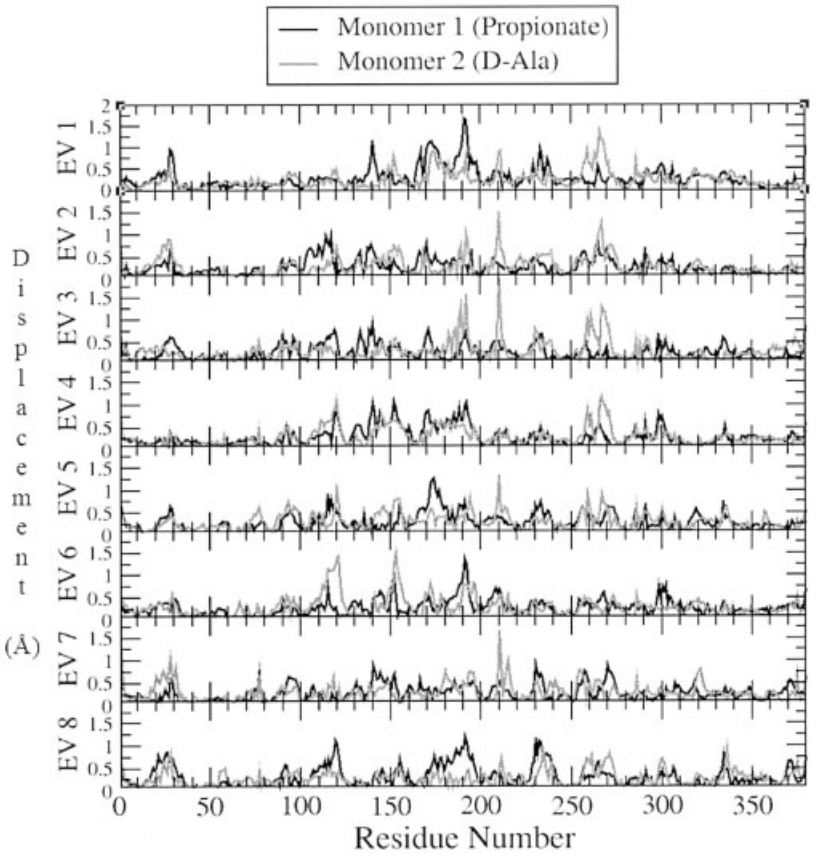

FIGURE 7 Absolute value of the components of the first eight eigenvectors (EV1–EV8) obtained from the C_α coordinate covariance matrix of the 1 ns trajectory as a function of residue number. Residues of the first monomer (propionate in the active site) are represented with a thick solid line; residues of the second monomer (D-Ala in the active site) are represented with a dashed line.

than the corresponding ones of the second monomer (D-Ala in the active site). This is another indication that the active site becomes more stabilized in the presence of the substrate.

In Figure 8 we illustrate the largest motions (colored in red) obtained from the ED analysis for both monomers [monomer 1 (propionate in the active site), left (A); monomer 2 (D-Ala in the active site), right (B)]. These motions were determined by averaging the displacement for each residue over the first eight eigenvectors. It is noticeable that a number of large deviations are observed in the first monomer (propionate in the active site) (Figure 8A) as compared to the second one (Figure 8B). These deviations occur in the N-terminal domain (α/β barrel), in particular, the α-helix H8 and the loop between α-helix H8 and β-strand B8 (indicated in Figure 8 as H8-B8). On the contrary, in the second monomer it is the C-terminal domain that displays larger displacements. These displacements occur in the short α-helix H10 and in the loop between β-strands B11–B12. Interestingly, Tyr 265′ is part of this loop and also displays larger displacements in the inhibitor-bound active site (0.48 Å) as compared to the substrate-bound active site (0.28 Å) (see Table VI). Therefore, the larger displacements that are observed for the loop bearing the catalytic base Tyr 265′ are also related to the presence of the inhibitor in the first active site.

CONCLUSIONS

Results obtained from a 2 ns MD simulation of the full AlaR homodimer from *B. stearothermophilus* (pdb code: 1SFT)[8] with a D-Ala molecule in one active site and the noncovalent inhibitor, propionate, in the second site are reported. The aim was to study the effects of substrate and inhibitor binding on the structure and flexibility of the protein and to analyze how the active site is affected by the presence of the substrate versus inhibitor.

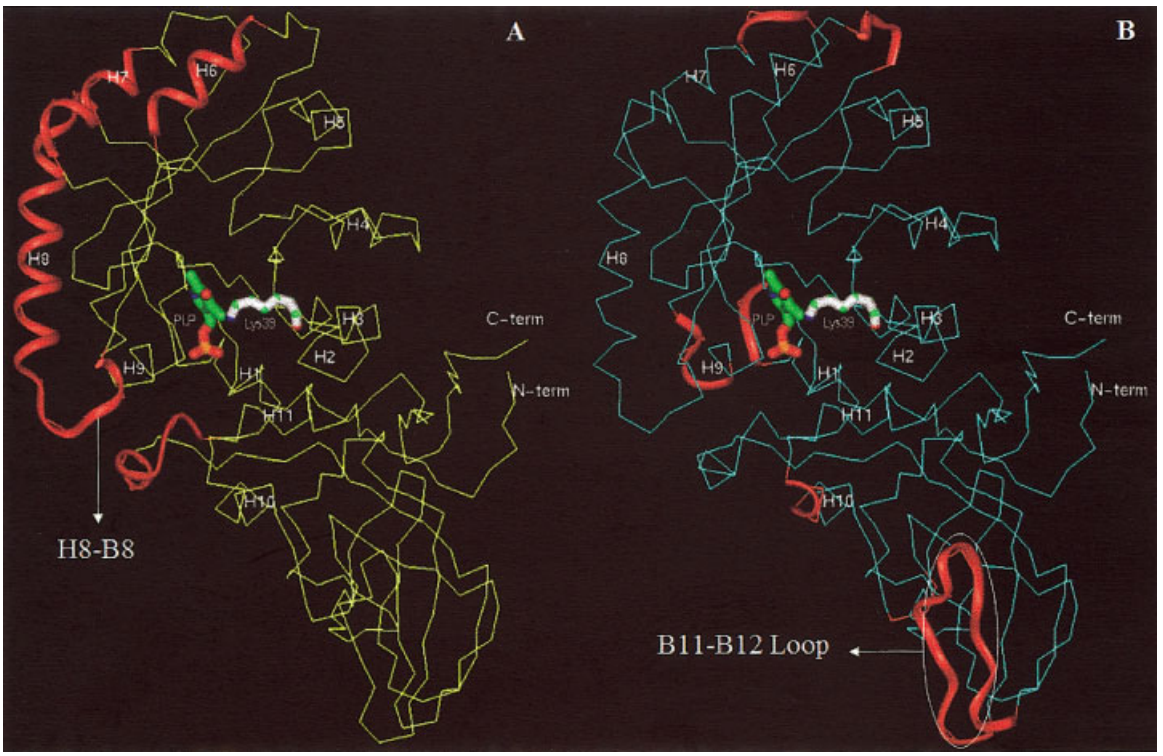

FIGURE 8 C_α trace and ribbon display of AlaR monomers. Monomer 1 (propionate in the active site) is displayed on the left side (A) and colored in yellow; monomer 2 (D-Ala in the active site) is displayed on the right side (B) and colored in turquoise; the PLP cofactor, colored by atom, and Lys 39 (white) are displayed in stick form. The motions obtained from the ED analysis that show the largest displacements are colored in red. The numbering of the α helices from the α/β barrel is in accordance with the one published by Shaw et al.[8]

Within the time scale of the simulation, we show that the second active site (D-Ala in the active site) becomes more stabilized in the presence of the substrate versus inhibitor. The results of this simulation are in agreement with the proposed mechanism of AlaRs[10] in which the substrate carboxyl group directly participates in the catalysis by mediating the proton transfer between the two catalytic bases, Lys 39 and Tyr 265′. The active site residues with the bound propionate are more flexible and the active site itself is larger as compared to the D-Ala bound active site.

Table VI Absolute Value of the Components (Å) Averaged over the First Eight Eigenvectors for the Most Important Active Site Residues

Residue	Active Site 1 (Propionate)	Active Site 2 (D-Ala)
Lys 39	0.18	0.14
Tyr 43	0.21	0.15
Lys 129	0.22	0.17
Arg 136	0.30	0.15
His 166	0.24	0.20
Arg 219	0.20	0.18
Tyr 265′	0.48	0.28
Met 312′	0.15	0.25
Asp 313′	0.22	0.16
Gln 314′	0.31	0.15
Tyr 354	0.17	0.18

A water molecule was identified in both active sites of the AlaR homodimer. This water molecule, in contact with both substrate and inhibitor and bridging residues in both active sites, shows a high-residence time in the simulation. For the future design of novel and specific inhibitors of AlaR, it may be important to take this structural water molecule into consideration by either utilizing it as a bridging group or displacing it with an inhibitor atom/group.

An ED analysis was performed to obtain a more detailed understanding of the flexibility of the active site upon substrate versus inhibitor binding. The results indicate that fluctuations in the region of the active sites are of differing magnitude, being larger in

the presence of inhibitor. Our results indicate that fluctuations in the α/β barrel are more substantial upon inhibitor binding with the α-helix H8 and the loop between α-helix H8 and β-strand B8 showing extensive flexibility. The N-terminal domain comprising a portion of the active site containing the substrate exhibits lesser fluctuations/displacements than the N-terminal domain in the active site containing the propionate inhibitor. Significant flexibility is observed in the C-terminal domain of the second monomer (substrate bound) and very little in the first monomer (inhibitor bound). This flexibility is also induced by inhibitor binding because this C-terminal domain faces the mouth of the α/β barrel of the first monomer (with propionate in the active site).

The present study provides insights into the dynamics of AlaRs in the presence of the substrate and an inhibitor, which are currently being used for studies involving rational drug design. The basic strategy is to use different conformations of the protein, taken at 100 ps intervals from our MD simulation, to generate a dynamic pharmacophore model using the property mapping capability of the LIGBUILDER program.[35] This pharmacophore model can be used for 3D database searching and compounds that fit our model will be considered as possible inhibitors of the enzyme.

METHODS

System Setup and MD Simulations

The protein structure used for the MD studies corresponds to *B. stearothermophilus* AlaR (pdb code: 1SFT),[8] containing acetate in each active site, from which we built a model with D-Ala in one active site and propionate in the second one. Propionate was modeled into the first active site by superimposing the *B. stearothermophilus* AlaR crystal structure in complex with the inhibitor propionate (pdb code: 2SFP)[6] on the first reported AlaR x-ray structure (pdb code: 1SFT).[8] The two structures are quite similar to each other, with a mean C_α RMSD of 0.29 Å. The substrate D-Ala was modeled in the second active site making use of the R-AlaR-1-aminoethylphosphonic acid (L-Ala-P) complex structure (pdb code: 1BD0),[9] which was superimposed on the same reference structure (pdb code: 1SFT).[8] The reason for using this structure in the modeling of D-Ala in the active site was because this was the first available x-ray structure to give a detailed description of the important interactions for binding and positioning of the substrate. Recently, two new crystal structures of *B. stearothermophilus* AlaR bound with reaction intermediate analogs, *N*-(5′-phosphopyridoxyl)-L-alanine (PLP-L-Ala) and *N*-(5′-phosphopyridoxyl)-D-alanine (PLP-D-Ala), became publicly available.[10] Our modeled D-Ala is in agreement with the new structures; that is, the α-hydrogen of the D-Ala points toward Lys 39 and the interatomic distances between the substrate and the two catalytic bases are 3.64 Å from C_α of D-Ala to the OH of Tyr 265′ and 3.30 Å from C_α of D-Ala to NZ of Lys 39.

The crystallographic studies performed by Shaw et al.[8] have suggested that the N1 atom of the PLP cofactor is bound with a basic amino acid (Arg 219), contrary to aminotransferases, which use a negatively charged amino acid (aspartate or glutamate) at the corresponding position. In AlaR, Arg 219 probably makes the pyridine nitrogen partially and less protonated than in L-aspartate aminotransferase, therefore destabilizing the quinonoid intermediate. Another interaction that involves the PLP cofactor and an active site side chain is the one between the NH2 of the guanidine side chain of Arg 136 and the hydroxyl group of the PLP. As suggested by Shaw et al.,[8] the NH2 of Arg 136 donates a hydrogen bond to the O6 alkoxide ion. According to the generally accepted AlaR reaction mechanism,[36,37] as well as on the basis of these crystallographic studies,[8] in our study we considered the pyridine nitrogen of the PLP to be protonated while the O6 hydroxyl group was modeled as unprotonated (i.e., in the alkoxide state).

Nevertheless, the recently determined x-ray structures of *B. stearothermophilus* AlaR in complex with the reaction intermediate analogues, N-(5′-phosphopyridoxyl)-L,D-alanine (PLP-L,D-Ala), suggest that both pyridine nitrogen (N2) and hydroxyl group (O6) of the cofactor seem to be protonated under normal catalytic conditions (pH 5–11).[10] On the contrary, based on the quantum chemical calculations performed by Watanabe et al. (2002), and in agreement with the site-directed mutagenesis studies performed by Sun and Toney (1999) it has been hypothesized that the pyridine nitrogen should be considered unprotonated because it interacts with a positively charged arginine (Arg 219). They do speculate, however, that the pyridine N is protonated. We believe that a more precise theoretical approach (e.g., combined quantum mechanics/molecular mechanics) should be employed in order to address this issue.

In order to obtain starting force field parameters for the PLP cofactor in its free (Figure 9) and lysine crosslinked forms, *ab initio* calculations were carried out. The bonded parameters assigned to the pyridoxal phosphate molecule were derived from pyridine rings and similar functional groups from the CHARMM22 force field.[20] The initial geometry was optimized at the MP2/6-31G* level and atomic charges were calculated by fitting to the electrostatic potential obtained from single point HF/6-31G* *ab initio* calculation with GAUSSIAN98[21] using the CHELPG protocol (Table VII).

Before the MD simulation was started, protonation states were predicted for all of the ionizable residues in the protein using the pK_a[22] procedure implemented in the UHBD program,[23] to determine whether any of the residues were likely to adopt nonstandard ionization states. Ondrechen et al. reported some unusual charge states for certain residues in the presence or absence of the cofactor.[11] However, on the basis of the results of these calculations in the presence

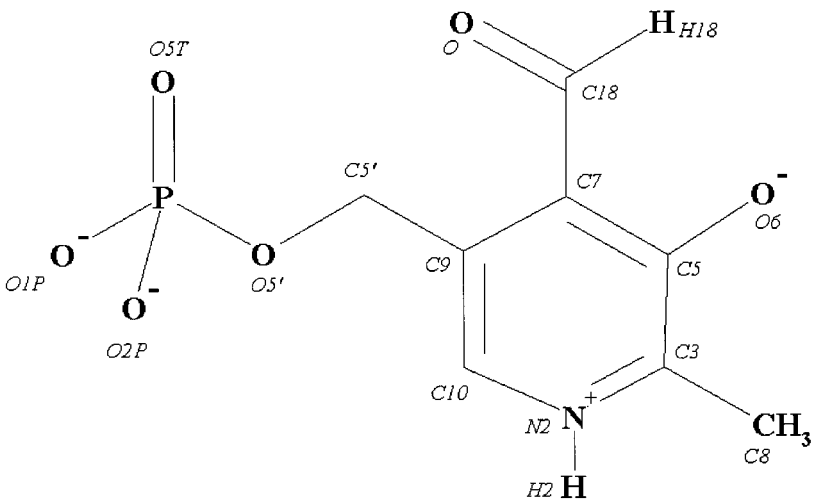

FIGURE 9 Two-dimensional structure of the PLP cofactor. The atom naming scheme used in the MD simulation is given in italic.

of crystal waters and with or without acetate, these residues were found to be close to their "free amino acid" ionization states and so were modeled accordingly.

The system was prepared and energy minimized using the CHARMM program.[24] The thermalization, equilibration, and the subsequent production phases were carried out using the NAMD program[25] in the NPT ensemble (pressure = 1 bar) with explicit solvent and periodic boundary conditions and a dielectric constant (ϵ) of 1. A constant temperature of 300 K was maintained by coupling to an external bath.[26] The protein and solvent interact via the CHARMM22 force field where all protein atoms are explicitly represented[20] and where water is characterized by the TIP3P model.[27] The hydrogen atoms were added using the HBUILD routine in CHARMM.

Bonds to hydrogen atoms were constrained using SHAKE[28] and the equations of motion were solved using the Verlet algorithm.[29] The simulation consisted of a system defined by the protein (762 residues; 12,137 atoms) plus the crystal waters (206 HOH; 618 atoms) and 15,943 solvent water molecules in a rectangular box of dimensions 76 $\times$ 106 $\times$ 76 Å. The total size of the system was 60,547 atoms. To avoid edge effects, periodic boundary conditions were used in the simulation. Long-range interactions were smoothly truncated at 10.5 Å with a shifting function for the electrostatic interaction and a switching function for the van der Waals interactions, the latter being applied between 9.5 and 10.5 Å. The nonbonded pairs list was updated every 10 steps. The truncation scheme applied to the calculation of electrostatic interactions was selected in order to reduce the computational effort and limit the perturbation induced by artificial periodicity imposed to the solution under periodic boundary conditions.[30] The observation that the conformations sampled in the protein trajectory depart little from the crystal structure supports the validity of our truncation scheme. However, recent studies have suggested that the Ewald summation method is a better protocol, at least for nucleic acids.[31] It has nevertheless also been shown to present a number of artifacts,[32,33] in particular when solute cavities are large compared to the unit cell, a feature characterizing our system.

The system was energy minimized with CHARMM with the following protocol. The whole system was constrained and subjected to 500 steps of steepest descent (SD) energy minimization. The solvent plus the substrate and the inhibitor were then relaxed and also subjected to 500 steps of SD energy minimization. Then the whole system was relaxed and minimized using SD for another 1000 steps. The entire system was then gradually heated, by means of temperature reassignment, from 50 to 300 K for 60 ps of MD. The whole system was then equilibrated for an additional 360 ps of MD at 300 K using a 2 fs time step, after which the system achieved stability. After the first 120 ps of MD (i.e., during the subsequent 300 ps of MD) a jump in the RMSD, from 0.5 to 0.75 Å, occurred as computed with respect to the minimized crystal structure. The subsequent production phase was performed in the NPT ensemble for 2 ns with a time step of 2 fs. Atomic coordinates were stored for later analysis every 0.5 ps.

Analysis of Structural Properties

RMSD. The RMSD of a selected element with respect to its reference value is defined as

$$RMSD = \sqrt{\frac{1}{N}\sum_{i=1}^{N}(\mathbf{r}_i - \mathbf{r}_0)^2} \qquad (1)$$

where $\mathbf{r}_i$ represents the element position at time i and $\mathbf{r}_0$ the reference value.

The mean-square fluctuation (MSF) of a selected element with respect to its average value is defined as

$$MSF = \frac{1}{N}\sum_{i=1}^{N}(\mathbf{r}_i - \langle \mathbf{r} \rangle)^2 \quad (2)$$

where $\mathbf{r}_i$ represents the element position at time i and $\langle r \rangle$ the average value.

B Factors. The isotropic temperature (B) factor was calculated from the MSF[15,34] using the equation

$$B = \frac{8\pi^2}{3}(MSF) \quad (3)$$

Secondary Structures. Secondary structure content was calculated using the DSSP software.[14]

Solvent Accessibility. The SASA of an amino acid side chain was computed with GROMACS 3.0[19] for every snapshot, averaged over the 2 ns trajectory, and normalized by a standard value of the corresponding residue computed from an extended Gly-XXX-Gly tripeptide.[16]

Hydrogen Bonds. Hydrogen bonds were identified using the CHARMM program[24] with the following criteria: a donor-acceptor distance must be $\leq$3.5 Å, and the donor-hydrogen-acceptor and the hydrogen-acceptor-"from" angles must be $\geq$90° ("from" stands for the atom covalently linked to the acceptor atom).

ED Analysis. To investigate functionally significant fluctuations in the protein, an ED analysis was performed on the 2 ns trajectory. The ED method[18] is based on the diagonalization of the covariance matrix built from atomic fluctuations in an MD trajectory from which overall translations and rotations have been removed. The covariance matrix is defined by

$$M_{ij} = \langle (x_i - x_{i,0})(x_j - x_{j,0}) \rangle \quad (4)$$

in which x_i and x_j are the separate X, Y, Z coordinates of the C_α atoms and x_0 are the average coordinates, the average being taken over the whole trajectory. Diagonalization of the covariance matrix yields a set of eigenvectors and eigenvalues, sorted by the size of eigenvalues. The eigenvectors indicate directions in the total configuration space, representing correlated displacements of groups of atoms in the system. The corresponding eigenvalues indicate the total MSFs, that is, the amplitude of the correlated motions along the trajectory. Only the correlated motions represented by the eigenvectors with large corresponding eigenvalues are significant for describing the overall motion of the protein.

Table VII Atomic Charges for the PLP Cofactor

Atom	Charge	Atom	Charge	Atom	Charge
N2	−0.63	C5	+0.13	H5′1	+0.09
H2	+0.42	O6	−0.64	H5′2	+0.09
C3	+0.38	C7	+0.12	O5′	−0.62
C8	−0.17	C18	+0.26	P	+1.50
H81	+0.05	H18	+0.04	O5T	−0.68
H82	+0.05	C9	−0.45	O1P	−0.82
H83	+0.05	C5′	−0.08	O2P	−0.82

This research was supported in part by NSF cooperative agreement ACI-9619020 through computing resources provided by the National Partnership for Advanced Computational Infrastructure at the Texas Advanced Computing Center. G. I. M. is grateful to Dr. I. J. Enyedy, A. Brigo, and Dr. H. -C. Huang for valuable assistance and fruitful discussions. Gratitude is expressed to the University of Houston High Performance Computing Center and the Texas Learning and Computation Center. Gratitude is also expressed to Accelrys, Inc. for providing software to us through the Institute for Molecular Design at the University of Houston.

REFERENCES

1. Wang, E.; Walsh, C. Biochemistry 1978, 17, 1313–1321.
2. Free, C. A.; Julius, M.; Arnow, P.; Barry, G. T. Biochim Biophys Acta 1967, 146, 608–610.
3. Duncan, K.; Faraci, W. S.; Matteson, D. S.; Walsh, C. T. Biochemistry 1989, 28, 3541–3549.
4. Patchett, A. A.; Taub, B.; Weissberger, M. E.; Valiant, M. E.; Gadebusch, H.; Thornberry, N. A.; Bull, H. G. Antimicrob Agents Chemother 1988, 32, 319–323.
5. Walsh, C. T. J Biol Chem 1989, 264, 2393–2396.
6. Morollo, A. A.; Petsko, G. A.; Ringe, D. Biochemistry 1999, 38, 3293–3301.
7. John, R.A. Biochim Biophys Acta 1995, 1248, 81–96.
8. Shaw, J. P.; Petsko, G. A.; Ringe, D. Biochemistry 1997, 36, 1329–1342.
9. Stamper, C. G. F.; Morollo, A.A.; Ringe, D. Biochemistry 1998, 37, 10438–10445.
10. Watanabe, A.; Yoshimura, T.; Mikami, B.; Hayashi, H.; Kagamiyama, H.; Esaki, N. J Biol Chem 2002, 277, 19166–19172.
11. Ondrechen, M. J.; Briggs, J. M.; McCammon, J. A. J Am Chem Soc 2001, 123, 2830–2834.
12. Strych, U.; Benedik, M. J. J Bacteriol 2002, 184, 4321–4325.
13. Carlson, H.A.; Masukawa, K.M.; Rubins, K.; Bushman, F.D.; Jorgensen, W.L.; Lins, R.D.; Briggs, J.M.; McCammon, J.A. J Med Chem 2000, 43, 2100–2114.

14. Kabsch, W.; Sander, C. Biopolymers 1983, 22, 2577–2637.
15. McCammon, J. A.; Harvey, S. Dynamics of Proteins and Nucleic Acids; Cambridge University Press: Cambridge, UK, 1987, pp. 96–105.
16. Engh, R. A.; Huber, R. Acta Crystallogr 1991, 47, 392–400.
17. Liang, J.; Edelsbrunner, H.; Woodward, C. Protein Sci 1998, 7, 1884–1897.
18. Amadei, A.; Linssen, A. B. M.; Berendsen, H. J. C. Proteins 1993, 17, 412–425.
19. Lindahl, E.; Hess, B.; van der Spoel, D. J Mol Model 2001, 7, 306–317.
20. MacKerell, A. D.; Bashford, D.; Bellott, M.; Dunbrack, R. L.; Evanseck, J. D.; Field, M. J.; Fischer, S.; Gao, J.; Guo, H.; Ha, S.; Joseph-McCarthy, D.; Kuchnir, L.; Kuczera, K.; Lau, F. T. K.; Mattos, C.; Michnick, S.; Ngo, T.; Nguyen, D. T.; Prodhom, B.; Reiher, W. E.; Roux, B.; Schlenkrich, M.; Smith, J. C.; Stote, R.; Straub, J.; Watanabe, M.; Wiorkiewicz-Kuczera, J.; Yin, D.; Karplus, M. J Phys Chem 1998, 102, 3586–3616.
21. Frisch, M. J.; Trucks, G. W.; Schlegel, H. B.; Scuseria, G. E.; Robb, M. A.; Cheeseman, J. R.; Zakrzewski, V. G.; Montgomery, J. A. J.; Stratmann, R. E.; Burant, J. C.; Dapprich, S.; Millam, J. M.; Daniels, A. D.; Kudin, K. N.; Strain, M. C.; Farkas, O.; Tomasi, J.; Barone, V.; Cossi, M.; Cammi, R.; Mennucci, B.; Pomelli, C.; Adamo, C.; Clifford, S.; Ochterski, J.; Petersson, G. A.; Ayala, P. Y.; Cui, Q.; Morokuma, K.; Malick, D. K.; Rabuck, A. D.; Raghavachari, K.; Foresman, J. B.; Cioslowski, J.; Ortiz, J. V.; Stefanov, B. B.; Liu, G.; Liashenko, A.; Piskorz, P.; Komaromi, I.; Gomperts, R.; Martin, R. L.; Fox, D. J.; Keith, T.; Al-Laham, M. A.; Peng, C. Y.; Nanayakkara, A.; Gonzalez, C.; Challacombe, M.; Gill, P. M. W.; Johnson, B.; Chen, W.; Wong, M. W.; Andres, J. L.; Gonzalez, C.; Head-Gordon, M.; Replogle, E. S.; Pople, J. A. GAUSSIAN 98; Gaussian, Inc.: Pittsburgh, PA, 1998. http://www.gaussian.com.
22. Antosiewicz, J.; Briggs, J. M.; Elcock, A. H.; Gilson, M. K.; McCammon, J. A. J Comput Chem 1996, 17, 1633–1644.
23. Madura, J. D.; Briggs, J. M.; Wade, R. C.; Davis, M. E.; Lutty, B. A.; Ilin, A.; Antosiewicz, J.; Gilson, M. K.; Bagheri, B.; Scott, L. R.; McCammon, J. A. Comp Phys Comm 1995, 91, 57–95.
24. Brooks, B. R.; Bruccoleri, R. E.; Olafson, B. D.; States, D. J.; Swaminathan, S.; Karplus, M. J Comp Chem 1983, 4, 187–217.
25. Kalé, L.; Skeel, R.; Bhandarkar, M.; Brunner, R.; Gursoy, A.; Krawetz, N.; Phillips, J.; Shinozaki, A.; Varadarajan, K.; Schulten, K. J Comput Phys 1999, 151, 283–312.
26. Berendsen, H. J. C.; Postma, J. P. M.; van Gusteren, N.F.; Di Nola, A.; Haak, J. R. J Chem Phys 1984, 81, 3684–3690.
27. Jorgensen, W. L.; Chandresekhar, J.; Madura, J.; Impey, R.; Klein, M. J Chem Phys 1983, 79, 926–935.
28. Ryckaert, J. P.; Cicotti, G.; Berendsen, H. J. C. J Comp Phys 1977, 23, 327–341.
29. Allen, M. P.; Tildesley, D. J. Computer Simulations of Liquids; Oxford University Press: New York, 1987, 78–82.
30. Wood, R. H. J Chem Phys 1995, 103, 6177–6184.
31. Sagui, C.; Darden, T. A. Annu Rev Biophys Biomol Struct 1999, 28, 155–179.
32. Hunenberger, P. H.; McCammon, J. A. J Chem Phys 1999, 110, 1856–1872.
33. Hunenberger, P. H.; McCammon, J. A. Biophys Chem 1999, 78, 69–88.
34. Brooks III, C. L.; Karplus, M.; Pettitt, B. M. Proteins: A Theoretical Perspective of Dynamics, Structure and Thermodynamics; Wiley-Interscience: New York, 1988; Vol. LXXI of Wiley Series on Advances in Chemical Physics, 192–193.
35. Wang, R.; Gao, Y.; Lai, L. J Mol Model 2000, 6, 498–516.
36. Faraci, W. S.; Walsh, C. T. Biochemistry 1988, 27, 3267–3276.
37. Kurokawa, Y.; Watanabe, A.; Yoshimura, T.; Esaki, N.; Soda, K. J Biochem 1998, 124, 1163–1169.
38. Sun, S.; Toney, M. D. Biochemistry 1999, 38, 4058–4065.
39. SAS, 8.1; SAS Institute Inc.: Cary, NC 27513, USA, 1999 http://www.sas.com